JOURNAL OF MATERIALS SCIENCE 24 (1989) 2081–2092

Ionic conductivity and crystal structure of fired crystalline zirconium phosphate completely and half exchanged with some monovalent cations

Y. SADAOKA, Y. SAKAI, M. MATSUGUCHI
Department of Industrial Chemistry, Faculty of Engineering, Ehime University, Matsuyama, 790 Japan

For LiLi-form, the decomposition of dilithium zirconium phosphate with a layered structure and formation of lithium dizirconium triphosphate and zirconium pyrophosphate was achieved by firing at 600° C or above. For NaNa- and KK-forms, any distinct variations of the external appearance were not confirmed by heat-treatments, while the crystal growth was detected for RbRb- and CsCs-forms fired at 900° C. For half ion-exchanged forms, monovalent cation dizirconium triphosphate was mainly formed on heating up to 600° C or above. The activation energy in ionic conduction decreases with increasing monovalent cation radius. This dependency can be realized by Anderson and Stuart's model based on the classical ideas of ionic crystal theory and elasticity theory. The activation energy for the fully exchanged form is slightly higher than that for the half-exchanged form and the pre-exponential factor in $\sigma T = \sigma_0 \exp(-E/kT)$ for the former is less than that for the latter.

1. Introduction

Zirconium phosphate is known as an insoluble inorganic ion exchanger and proton conductor [1–3]. In zirconium *bis*(monohydrogen phosphate) monohydrate, the structure of which is well known, each layer consists of a plane of zirconium atoms bridged through tetrahedral phosphate groups located alternatively above and below in this plane. Because the acidic protons of this material are easily exchanged by small cations such as Li^+, Na^+, K^+ etc., and the degree of ion exchange can be controlled by the regulation of pH in zirconium *bis*(monohydrogen phosphate) monohydrate-dispersed solution, the obtained alkali salt is known as an ionic conductor [4, 5]. The electrical properties of these alkali salts have been reported by some workers. Casciola and Fabiani [5] have reported that the conductivity in the temperature range 150 to 350° C increases with decreasing ionic radius of the alkali ion and its activation energy is estimated to be 0.68 eV for the LiLi-form, 0.72 eV for the NaNa-form and 0.94 eV for the KK-form. In addition, Dyer and Ocon [6] have reported that the activation energy in cation self diffusion is 0.66 eV for Na^+, 0.72 eV for K^+ and 0.86 eV for Cs^+, respectively. From these reported results, it is clear that the alkali salts act as cation conductors. Previously, we have reported that the sintered dilithium zirconium phosphate was a good ionic conductor and its electrical conductivity was comparable to LiI, $Li_{1.4}Zn(GeO_4)_4$ and $Li_{3.6}Si_{0.6}P_{0.4}O_4$ [7]. It seems that zirconium *bis*(monohydrogen phosphate) is a suitable material as a starting reagent to prepare an ionic conductor. In the present paper, the morphology, crystal structure and electrical conductivity of fired fully and half ion-exchanged zirconium phosphates were examined.

2. Experimental details

Zirconium *bis*(monohydrogen phosphate) monohydrate was prepared by the refluxing of amorphous zirconium phosphate with excess of phosphoric acid for 100 h. Alkali salt was obtained by titrating zirconium *bis*(monohydrogen phosphate) monohydrate suspended in distilled and deionized water for Li-, Na- and K-forms and in purified water with small amounts of sodium ion for Rb-, Cs- and Ag-forms with the corresponding alkali hydroxide solution. The degree of ion exchange was determined by titration with sodium hydroxide solution. Fully and half ion-exchanged samples are denoted X_2- and XH-form (X = monovalent cation), respectively. All the products were washed with purified water and dried at 60° C. The dried powder was pressed into a disc at 200 kg cm^{-2} and the disc, ~0.5 mm thick, was then shaped to 10 mm × 10 mm. This was then heated at various temperatures. The gold electrodes, 4 mm × 4 mm, were applied to both faces of the disc by vacuum evaporation.

Electrical properties were measured by the a.c. method in the frequency region 100 Hz to 100 kHz in a nitrogen flow (40 ml min^{-1}) from 100 to 600° C. The structure and external appearances were examined by the standard X-ray diffraction technique (XRD) and scanning electron microscopy (SEM), respectively.

0022–2461/89 $03.00 + .12

TABLE I Ionic composition and water losses

Form	Water loss			
	Cavity water		Condensation water	
	Mole	Approximate temperature range (°C)	Mole	Approximate temperature range (°C)
HH	1.0	150	1.0	550
LiLi	1.3	300		
NaNa	1.1	200		
KK	1.0	150		
RbRb	1.1	150	0.01	600
CsCs	1.6	150	0.06	620
LiH	2.3	150	0.42	500
	0.9	400		
NaH	0.9	150	0.51	500
KH	0.3	250	0.56	600
AgH	1.3	250	0.58	450

3. Results and discussion

3.1. Structure and external appearances

3.1.1. Fully ion-exchanged samples

The starting material was identified as zirconium *bis*(monohydrogen phosphate) monohydrate with layered structure by titration, thermogravimetry (TG) and XRD. As is well known, most of the crystals contain some cavity water, and weight loss in thermogravimetry is caused by the release of cavity water and of condensation water. In Table I, the characteristic temperatures of weight loss in both procedures are summarized. The release of cavity water was achieved by heating up to ~300° C and the condensation occurred at ~600° C. The discs were fired at 60, 300, 600 and 900° C. The external appearances were examined by SEM and XRD and the results are shown in Figs 1 and 2 and in Tables II and III.

For the LiLi-form fired at 600° C or below, the external appearances were almost independent of firing temperature and the layered structure was retained. By heating to 900° C, some deformation was detected i.e. diminishing layer structure and the change of phase were confirmed. The results of XRD are indicated in Table II for the LiLi-forms. For the sample dried at 60° C, the strong and weak peaks were detected at $d = 0.790$ and 0.876 nm, respectively, and the former suggest the existence of monohydrate and the latter dihydrate in which the observed d-values correspond to the interlayer distance. By heating up to 300° C, the interlayer distance is lowered to 0.703 nm which means the complete release of the cavity water. In addition, for the sample fired at 600 and 900° C, the weak peak observed at $d = 0.633$ and 0.622 nm, respectively, was assigned to the interlayer distance. The temperature dependence of the interlayer distance confirmed in this work was in fairly good agreement with the results published by other workers [8]. For the sample fired at 600 and 900° C, some new strong diffraction peaks were confirmed at $d = 0.443$ nm

TABLE II XRD patterns

Form	60° C				300° C				600° C				900° C			
	d (nm)	I/I_0	d (nm)	I/I_0	d (nm)	I/I_0	d (nm)	I/I_0	d (nm)	I/I_0	d (nm)	I/I_0	d (nm)	I/I_0	d (nm)	I/I_0
H_2	0.756	63	0.262	30	0.750	100			0.656	67			0.478	33	0.249	41
	0.447	43			0.452	41			0.452	100			0.414	100		
	0.355	100			0.360	56							0.369	35		
	0.352	56											0.337	32		
	0.264	30			0.264	33			0.267	67			0.292	32		
Li_2	0.876	20	0.358	76	0.808	5	0.363	100	0.633	6	0.334	14	0.622	5	0.376	31
	0.790	100	0.352	54	0.703	80	0.325	10	0.564	11	0.314	37	0.561	15	0.335	19
	0.446	43	0.324	20	0.454	30	0.294	46	0.443	100	0.309	14	0.442	100	0.313	45
	0.433	22	0.273	15	0.433	11	0.274	16	0.398	16	0.275	14	0.396	21	0.309	24
	0.363	67	0.267	17	0.384	34	0.242	17	0.379	42	0.255	37	0.379	31	0.275	21
Na_2	0.847	100	0.359	47	0.859	100	0.334	24	0.859	100	0.299	38	0.763	100	0.387	79
	0.456	27	0.296	17	0.455	44	0.323	12	0.456	36	0.293	10	0.436	83	0.379	75
	0.445	60	0.279	13	0.445	11	0.298	42	0.416	26	0.267	25	0.430	67	0.366	35
	0.388	50	0.267	13	0.416	35	0.267	33	0.388	63	0.254	25	0.420	38	0.350	54
	0.363	67	0.262	40	0.388	82	0.254	32	0.334	23			0.390	75	0.339	62
K_2	0.893	89	0.353	58	0.903	53			0.898	48			0.907	56		
	0.461	37	0.319	58			0.319	100			0.319	100			0.319	100
	0.433	58	0.302	95												
	0.403	42			0.403	78			0.402	73			0.403	78		
	0.391	100														
Rb_2	0.912	18	0.307	15	0.917	19	0.308	16	0.912	15	0.307	15	0.912	20		
	0.414	31	0.266	69	0.416	33	0.267	72	0.413	36	0.266	81	0.431	16	0.266	46
	0.407	41	0.211	13	0.409	42	0.211	13	0.408	42	0.210	15	0.410	63		
	0.329	100	0.204	26	0.330	100	0.204	28	0.329	100	0.204	28	0.324	100	0.205	35
	0.318	38			0.319	33			0.319	38			0.296	21		
Cs_2	0.441	20	0.316	20	0.460	10	0.351	100	0.466	15	0.364	46	0.470	10	0.314	19
	0.374	50	0.271	40	0.439	24	0.337	71	0.441	31	0.352	100	0.427	77	0.298	100
	0.351	100	0.257	20	0.419	33	0.317	38	0.421	54	0.342	62	0.419	54	0.271	46
	0.342	70	0.220	20	0.389	10	0.271	38	0.393	15	0.334	100	0.381	35	0.247	23
	0.333	40			0.373	48	0.269	43	0.375	69	0.318	38	0.332	94	0.213	25

TABLE III XRD patterns

Form	60° C				300° C				600° C				900° C			
	d (nm)	I/I_0	d (nm)	I/I_0	d (nm)	I/I_0	d (nm)	I/I_0	d (nm)	I/I_0	d (nm)	I/I_0	d (nm)	I/I_0	d (nm)	I/I_0
LiH	1.01	100	0.407	67	1.01	34	0.405	57	0.477	24	0.336	36			0.336	39
	0.864	19	0.387	33	0.862	69	0.386	45	0.441	100	0.314	43	0.441	100	0.314	47
	0.455	40	0.352	54	0.758	72	0.376	66	0.413	78	0.291	24	0.413	89	0.291	25
	0.431	59	0.239	55	0.454	100	0.369	83	0.378	25	0.255	27	0.378	28	0.255	30
	0.418	49	0.229	50	0.423	51	0.261	82	0.369	31	0.249	31	0.369	32	0.249	33
NaH	0.787	89	0.377	53	0.725	66	0.293	17	0.634	23	0.287	90	0.635	27	0.287	88
	0.457	29	0.349	54	0.458	34	0.275	29	0.457	68	0.258	20	0.457	76	0.257	22
	0.432	46	0.315	71	0.398	36	0.268	15	0.441	96	0.254	40	0.440	99	0.254	40
	0.414	100	0.268	39	0.376	100	0.257	19	0.381	100	0.202	18	0.381	100	0.202	20
			0.254	26	0.298	10	0.251	10	0.317	46			0.317	57		
KH	0.760	67	0.346	17	0.758	58	0.316	20	0.639	23	0.294	100	0.639	21	0.294	100
	0.460	46	0.316	22	0.460	51	0.304	13	0.469	41	0.283	10	0.469	40	0.283	10
	0.420	31	0.282	19	0.420	29	0.282	22	0.436	88	0.251	32	0.436	85	0.251	32
	0.381	100	0.264	24	0.381	100	0.264	28	0.383	77	0.227	10	0.383	73	0.213	15
	0.357	12	0.215	14	0.346	16	0.215	14	0.319	41	0.213	16	0.319	37	0.206	10
AgH	0.744	100	0.333	16	0.723	10	0.360	34	0.477	32	0.337	16	0.477	22	0.337	28
	0.445	32	0.292	16	0.459	100	0.295	32	0.442	65	0.292	44	0.441	100	0.291	41
	0.376	18	0.283	11	0.441	36	0.291	50	0.412	100	0.288	67	0.412	78	0.288	96
	0.354	97	0.264	34	0.395	42	0.276	76	0.383	33	0.255	23	0.382	52	0.255	37
	0.351	51	0.261	25	0.378	56	0.260	34	0.369	39	0.249	40	0.369	28	0.249	33

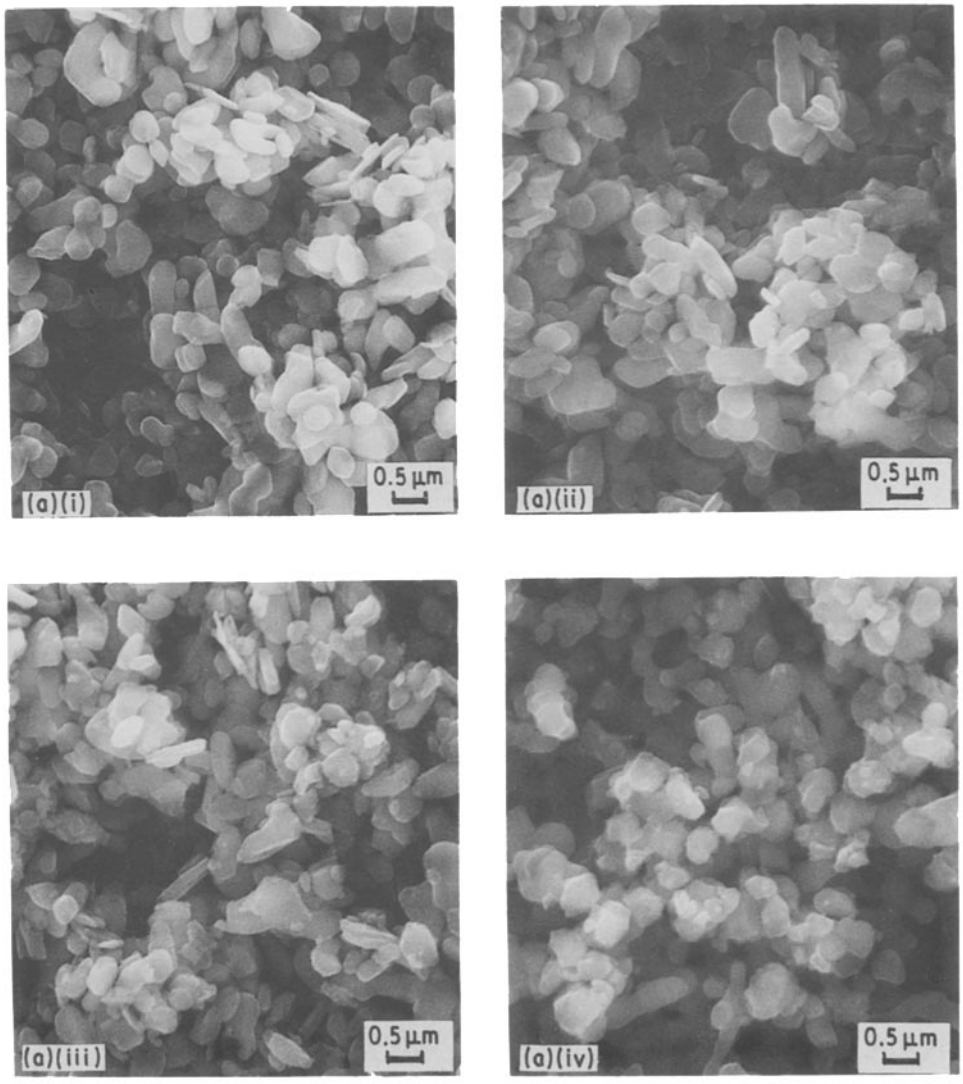

Figure 1 Scanning electron micrographs of (a) LiLi-, (b) NaNa-, (c) KK-, (d) RbRb- and (e) CsCs-forms. Firing temperature: (i) 60° C, (ii) 300° C, (iii) 600° C, (iv) 900° C.

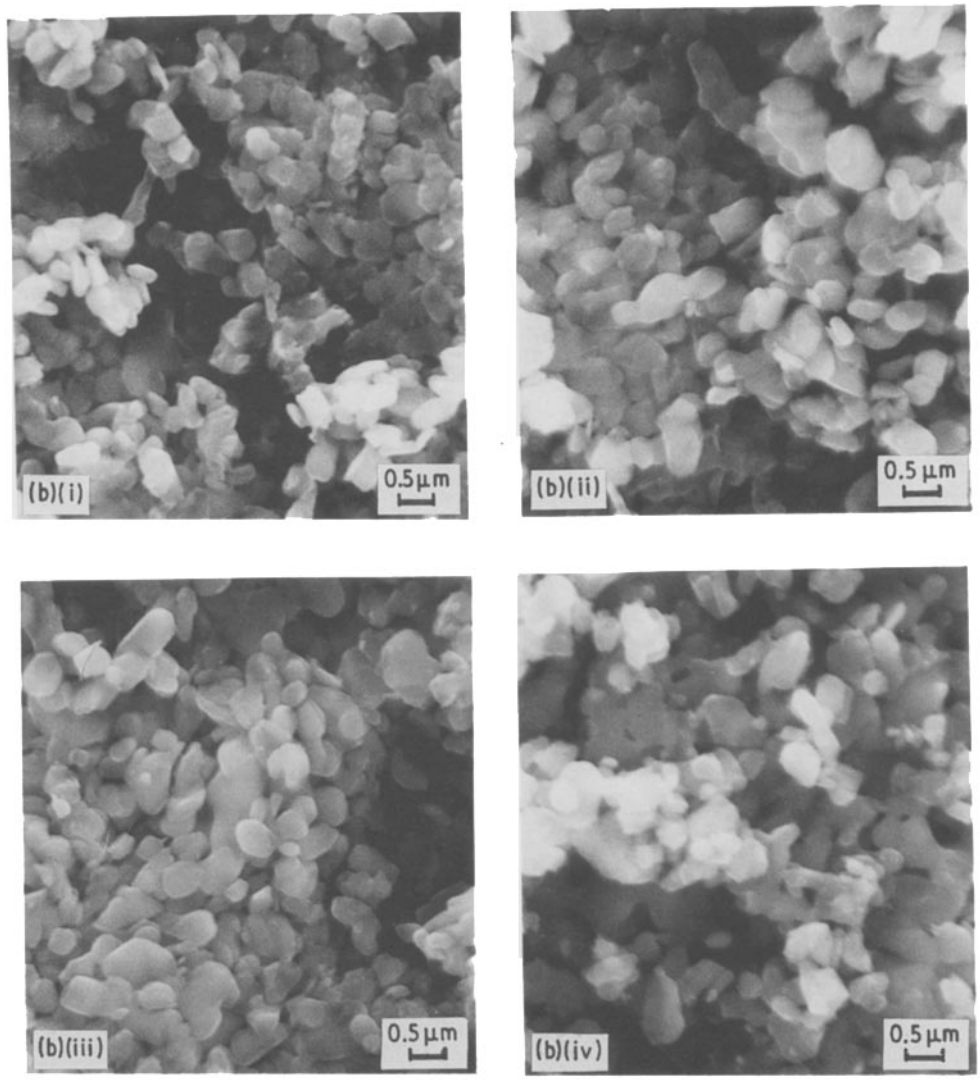

which has a shoulder in a higher d-value side and at $d = 0.314$ nm. These new peaks were assigned to lithium dizirconium triphosphate, while the existence of zirconium pyrophosphate could not be confirmed. The observed results may be summarized as

$$Zr(LiPO_4)_2 \cdot 1.3H_2O \xrightarrow{300^\circ C}$$

$$Zr(LiPO_4)_2 \xrightarrow{600^\circ C} LiZr_2(PO_4)_3$$

$$+ \text{ unknown } + Zr(LiPO_4)_2$$

While it is difficult to determine the unknown compounds, the formation of trilithium phosphate is presumed by the appearance of the new peaks in XRD at $d = 0.398$ and 0.380 nm.

While no distinct deformations were observed for the NaNa-form fired at or below 600° C, some sintering (interparticle fusion) was confirmed for the sample fired at 900° C. For the KK-form, no distinct sintering and/or deformations were observed even for the sample fired at 900° C. For the NaNa-form fired at or below 600° C, the strong diffraction peak at $d = 0.847$ to 0.859 nm which could be assigned to the interlayer distance, was confirmed and the XRD patterns (Table II) indicate that any apparent deformations in the crystal structure were not induced by the heat treatment up to 600° C while the release of the cavity water is achieved by heating at ~200° C. On the other hand, on increasing the firing temperature to 900° C, a decrease in the interlayer distance to 0.763 nm was observed and most of the observed diffraction peaks were assigned to sodium zirconium phosphate.

$$Zr(NaPO_4)_2\ 1.1H_2O \xrightarrow{200^\circ C} Zr(NaPO_4)_2$$

In addition, the temperature dependence of the structure of KK-form is expressed as

$$Zr(KPO_4)_2\ 1.1H_2O \xrightarrow{150^\circ C} Zr(KPO_4)_2$$

On the other hand, a distinct deformation of the external appearance was confirmed for RbRb- and CsCs-forms. Firstly, it seems that the crystallinity of the samples dried at 60° C was considerably lowered by exchange of protons with Rb^+ or Cs^+ ions. Furthermore, the crystallinity and size of the crystals increased with increasing firing temperature, and in particular, a distinct crystal growth was confirmed for the samples fired at 900° C and the layer structure might be retained because the anisotropies in crystal

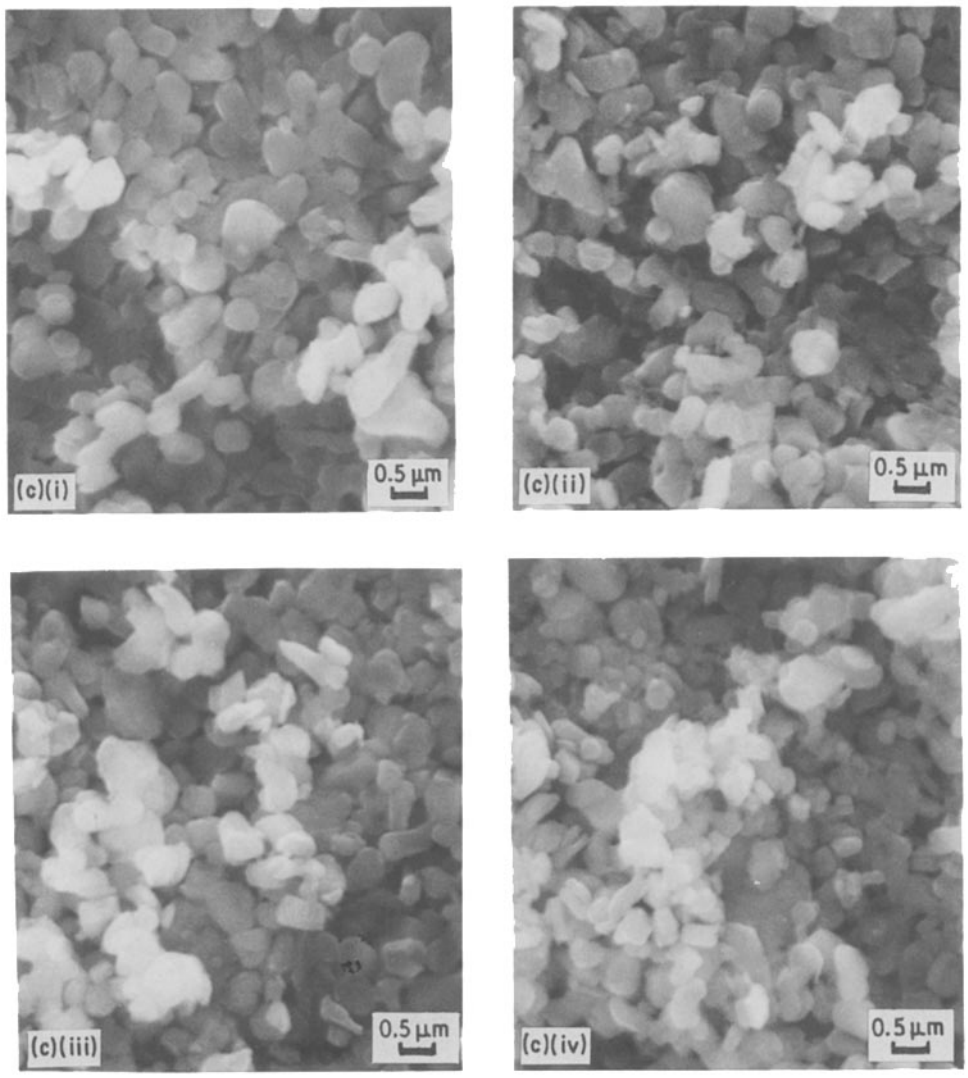

Figure 1 Continued.

growth were observed as shown in Figs 1e and f. To examine this in more detail, the crystal structure was studied by XRD. The results are indicated in Table II. For the RbRb-form, the weak diffraction peak at $d = 0.912$ nm, which corresponds to the interlayer distance, was confirmed for all samples. This d-value is comparable to the results reported by Alberti and Constantino [8]. In addition, the XRD patterns were little influenced by the firing temperature while the external appearances were distinctly affected. These observed results are interpretable in terms of the crystal growth by increasing the firing temperature and, in fact, the relative intensity of the diffraction peaks increases with increasing firing temperature. For the CsCs-form, the relative intensity of the diffraction peaks for the sample fired at or below 600° C was very weak while distinct sharp diffraction peaks were observed for the sample fired at 900° C. These tendencies are consistent with the external appearances. Unfortunately, the observed diffraction patterns were not consistent with the published results. Alberti and Constantino [8] reported that the well crystalline phase with a layered structure could be prepared by a similar preparation procedure. It seems that the discrepancy is caused by the difference of the crystal size of zirconium *bis*(monohydrogen phosphate) as a starting material, but, at the present stage, it is difficult to discuss in more detail.

3.1.2. Half ion-exchanged samples

The XRD pattern excepting the peak at $d = 0.86$ nm for the LiH-form dried at 60° C, was assigned to $ZrLiH(PO_4) \cdot 4H_2O$, while the amount of cavity water was 3.2 and slightly lower. This difference may be caused by the existence of a dehydrated form. For the sample fired at 300° C, the main product is composed of $ZrLiH(PO_4) \cdot H_2O$. On heating up to 600° C or above, the proton is completely removed as water, and the XRD patterns indicate the formation of ZrP_2O_7 and $LiZr_2(PO_4)_3$. That is,

$$ZrLiH(PO_4)_2 \cdot 3.2H_2O \xrightarrow{150^\circ C} ZrLiH(PO_4)_2 \cdot H_2O$$

$$\xrightarrow{\sim 600^\circ C} LiZr_2(PO_4)_3 + ZrP_2O_7$$

For the NaH-form, the cavity water was completely released at 150° C and the condensation of water occurred at 500° C as shown in Table I. The observed XRD patterns are comparable to the TG results and, in conclusion, the change of the composition is

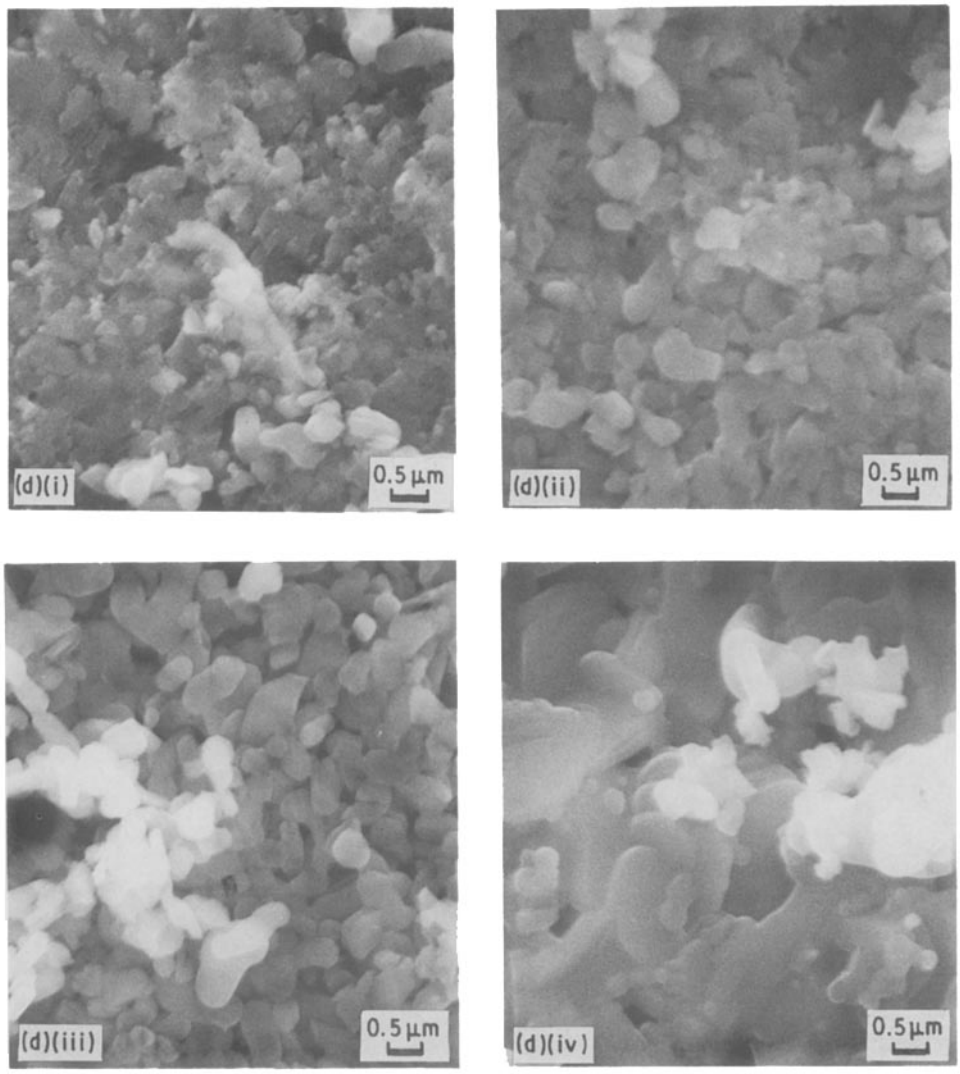

expressed as

$$ZrNaH(PO_4)_2 \cdot 0.9H_2O \xrightarrow{150^\circ C} ZrNaH(PO_4)_2$$

$$\xrightarrow{500 \text{ to } 600^\circ C} NaZr_2(PO_4)_3$$

In this system, the formation of ZrP_2O_7 could not be detected even for the sample fired at 900° C.

For the KH-form, the composition of the sample fired at 300° C or below was assigned to $ZrKH(PO_4)_2$ and the formation of only $KZr_2(PO_4)_3$ was confirmed for the sample fired at 600 and 900° C.

$$ZrKH(PO_4)_2 \cdot 0.3H_2O \xrightarrow{250^\circ C} ZrKH(PO_4)_2$$

$$\xrightarrow{\sim 600^\circ C} KZr_2(PO_4)_3$$

The XRD patterns observed for the AgH-form fired at 300° C and below, are similar to the KH-form. The *d*-value (0.744 nm) observed for the sample dried at 60° C is slightly higher than that for the KH-form, despite the fact that the ionic radius of the Ag^+ ion is slightly smaller than that of the K^+ ion. This discrepancy may be caused by the difference in the number of cavity water molecules, i.e. the number of cavity water molecules for the AgH-form is 1.3, and higher than that for the KH-form (0.3). For the sample fired at 600° C or above, the formation of ZrP_2O_7 and $AgZr_2(PO_4)_3$ was detected. Similar results have been reported by Ginestra *et al.* [9]. The change in composition with heat-treatment is expressed as

$$ZrAgH(PO_4)_2 \cdot 1.3H_2O \xrightarrow{250^\circ C} ZrAgH(PO_4)_2$$

$$\xrightarrow{450 \text{ to } 600^\circ C} AgZr_2(PO_4)_3 + ZrP_2O_7$$

While the formation of monocation dizirconium triphosphate is detected by XRD for the half-exchanged sample fired at 600° C, no distinct variations in external appearance is confirmed. However, by increasing the firing temperature up to 900° C, drastic deformations of the external appearance were confirmed as shown in Figs 2a to d and the intensity of the diffraction peaks increased.

3.2. Electrical properties

The frequency dependence of impedance was examined in the frequency region 100 Hz to 100 kHz and the conductivity was determined by a complex impedance analysis. In each case the ionic conductivity is therm-

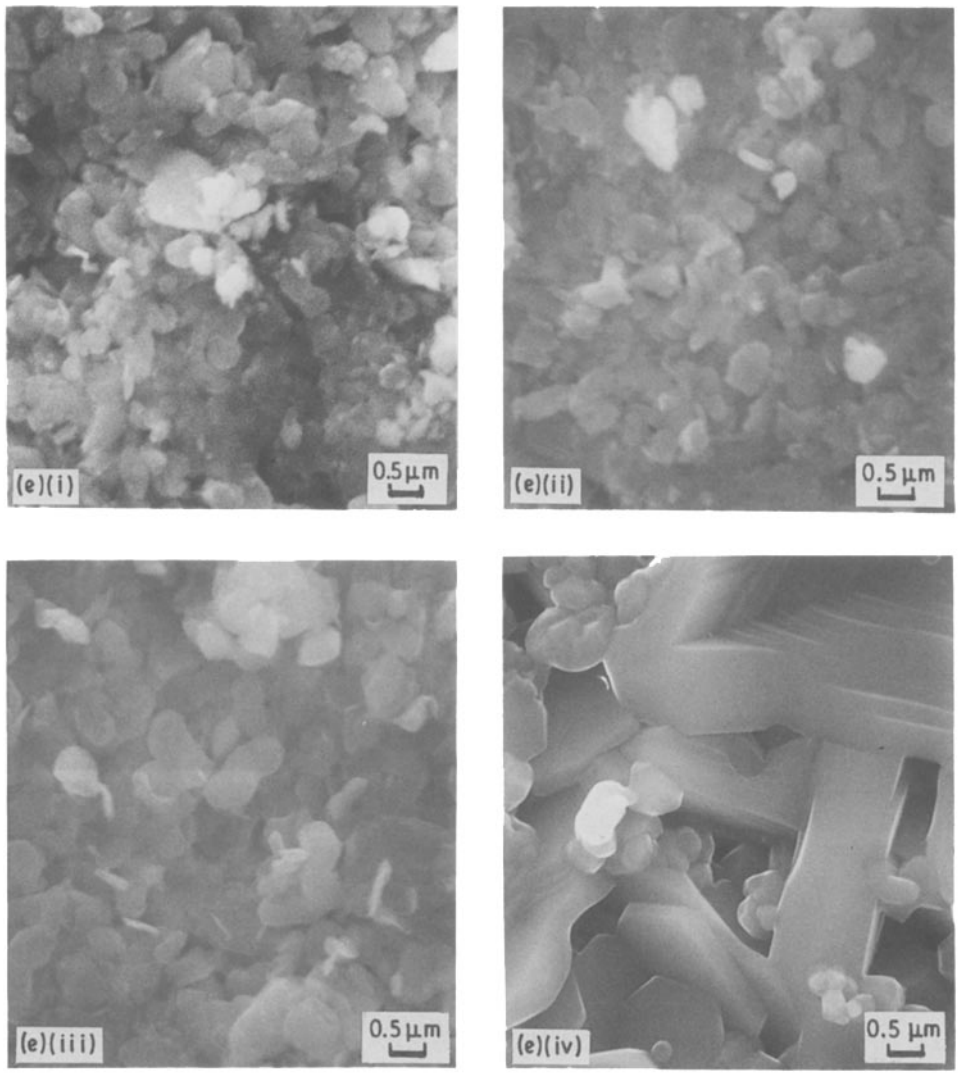

Figure 1 Continued.

ally activated and may be represented by the expression

$$\sigma T = \sigma_0 \exp(-E/kT) \quad (1)$$

in which E is the activation energy, k is Boltzmann's constant and T is absolute temperature.

For example, the correlation between log σT and $1/T$ for the samples fired at 600° C is shown in Fig. 3. In Table IV, the logarithm of the pre-exponential factor, σ_0, and the activation energy in conduction are given. For all samples, the electrical measurements were taken in the temperature range below the pre-heat-treatment temperature to prevent any phase transition or decomposition in the discs during the measuring procedures. For fully ion-exchanged samples, except the LiLi-form fired at 600 and 900° C, the correlation between log σT and $1/T$ is expressed by a straight line with no apparent deviations. For LiLi-, NaNa- and KK-forms fired at 300° C, the activation energy in conduction is in good agreement with that published for conduction and the diffusion coefficient determined radiochemically [5, 6]. The correlation between the activation energy and ionic radius of the monovalent cation is shown in Fig. 3 for fully ion-exchanged samples. For the LiLi-form in particular, the activation energy decreases from 0.69 to 0.47 eV on increasing the firing temperature up to 600° C. Furthermore, for the LiLi-form fired at 900° C, the activation energy estimated from the lower temperature range below ~270° C is 0.79 eV, and is higher than that for the LiLi-form fired at 600° C; some differences in the external appearance were confirmed while no distinct differences in XRD patterns were detected.

Recently, Petit *et al.* [10] prepared lithium dizirconium triphosphate by a sol/gel route and following the heat-treatment. In addition, they confirmed a curvature in the log σT–$1/T$ relation at ~280° C and this point was correlated to the phase transition from monoclinic to rhombohedral. The characteristics reported by Petit *et al.* are comparable to the results for the LiLi-form fired at 900° C. For the NaNa- and KK-forms, the activation energy decreases with increasing firing temperature while its dependency is small. As mentioned above, the crystal structure and its size are little influenced by the firing temperature and also the interlayer distance. On the other hand, for the RbRb- and CsCs-forms, the activation energy increases on heating to 900° C, while the XRD patterns are little influenced by increasing the firing temperature

TABLE IV Electrical properties of fired samples

Firing temperature (° C)	Form	E (eV)	log σ_0 (S cm^{-1} K)	Form	E (eV)	log σ_0 (S cm^{-1} K)
300	HH	0.80	3.46	CsCs	–	–
600	HH	0.84	1.17	CsCs	0.94	3.40
900	HH	0.83	0.41	CsCs	1.23	5.64
300	LiLi	0.69	4.39	LiH	0.81	5.95
600	LiLi*	0.56	4.02	LiH‖	0.83	7.06
600	LiLi†	0.46	3.15	LiH¶	0.45	3.99
900	LiLi‡	0.79	6.56	LiH‖	0.95	8.09
900	LiLi§	0.42	3.20	LiH¶	0.56	4.78
300	NaNa	0.69	4.04	NaH	0.76	3.69
600	NaNa	0.68	2.75	NaH	0.75	4.03
900	NaNa	0.66	3.25	NaH	0.67	4.15
300	KK	0.90	4.39	KH	0.78	2.42
600	KK	0.85	3.37	KH	1.03	5.43
900	KK	0.79	3.54	KH	1.38	7.49
300	RbRb	–	–	AgH	0.64	3.51
600	RbRb	0.91	3.27	AgH	0.56	4.43
900	RbRb	0.98	4.31	AgH	0.67	5.87

* < 210° C, † > 210° C, ‡ < 270° C, § > 270° C, ‖ < 330° C, ¶ > 330° C.

from 600 to 900° C, i.e. it seems that the crystal structure is the same. However, as shown, by increasing the firing temperature, the external appearances are distinctly changed, i.e. a distinct crystal growth is induced.

For half ion-exchanged forms, the correlation between the activation energy and ionic radius of monovalent cation is shown in Fig. 4. Two activation energies are estimated in a higher and a lower temperature range, especially for the LiH-form fired at 600 and 900° C, while only one value was obtained for that fired at 300° C. Similar behaviour has been confirmed in the LiLi-form. For the LiH-form fired at 600° C or above, the formation of lithium dizirconium triphosphate with zirconium pyrophosphate is confirmed. For NaH- and AgH-forms, no apparent dependency of the firing temperature on the activation energy was detected, while the value increased distinctly with the firing temperature, especially for the KH-form.

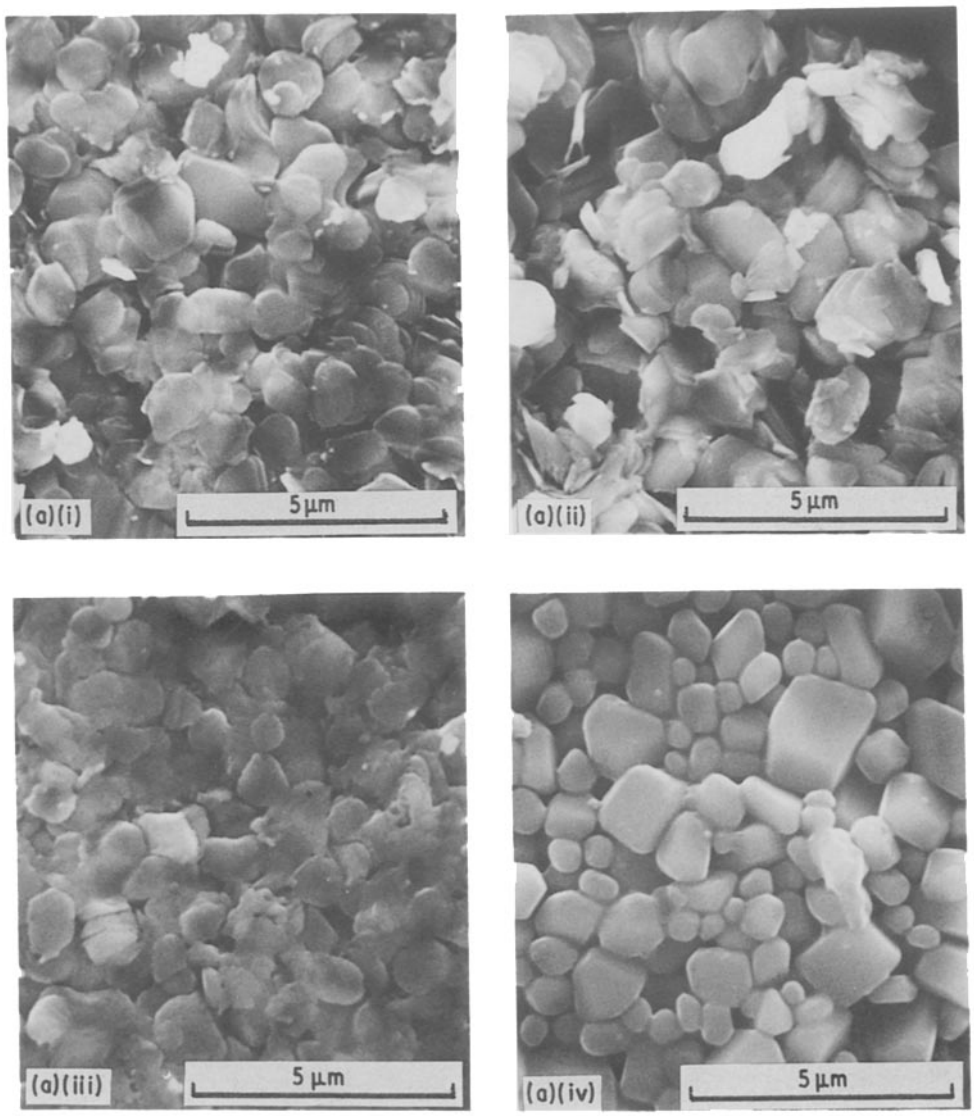

Figure 2 Scanning electron micrographs of (a) LiH-, (b) NaH-, (c) KH- and (d) AgH-forms. Firing temperature: (i) 60° C, (ii) 300° C, (iii) 600° C, (iv) 900° C.

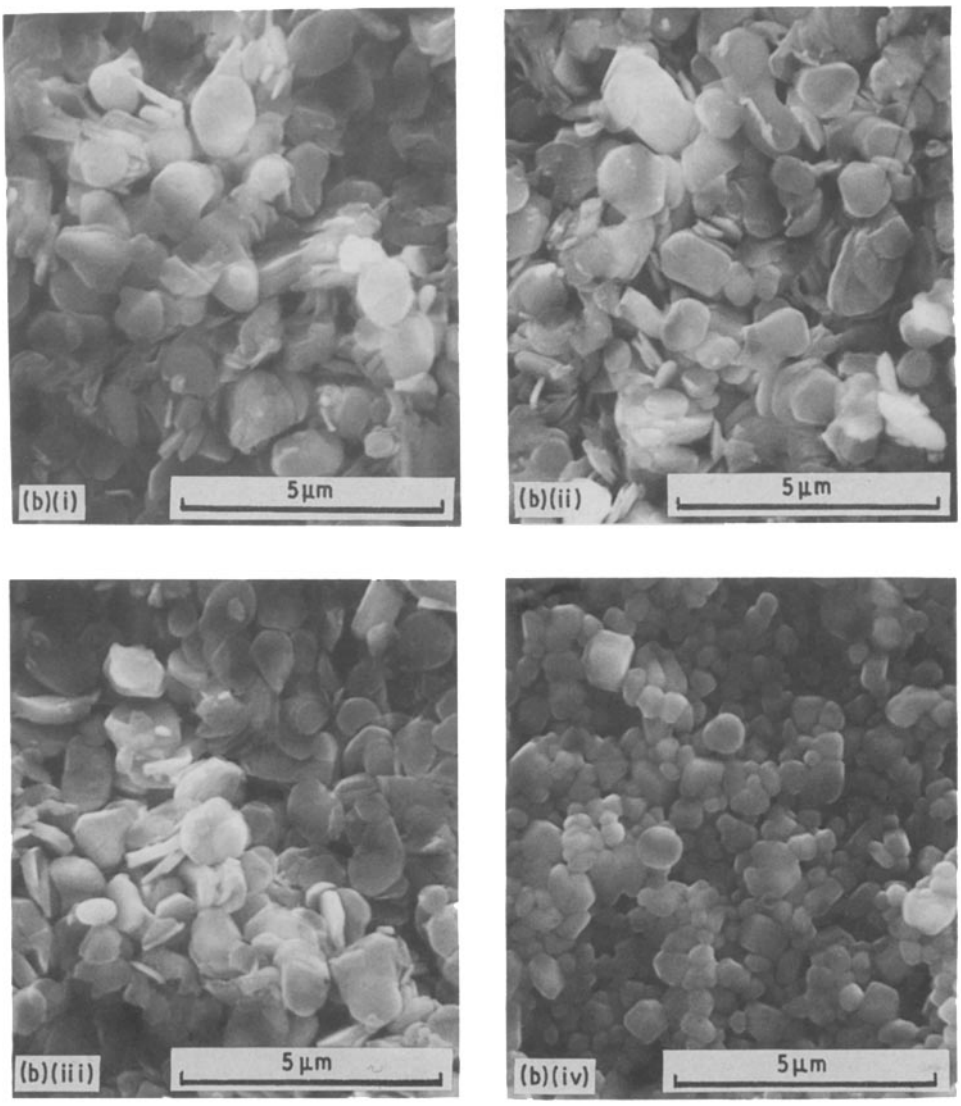

Figure 2 Continued.

According to Anderson and Stuarts model [11] for ionic conductivity, the activation energy of ionic conduction is the sum of the electrostatic energy change and the energy required to move the ion

$$E = \beta Z Z_0 e^2/\gamma(r + r_0) + 4\pi G r_D(r - r_D)^2 \quad (2)$$

where Z and Z_0 are the valence of the ion pair, r and r_0 are the radii of cations and anions, β is the finite displacement factor, γ accounts for the deformability of the oxygen atom, G is the shear modulus and r_D is the characteristic radius. While it is difficult to estimate some unknown characteristics, it is realized that the activation energy is strongly affected by the ionic cation species. In this case, it is assumed that the monovalent cation binds with the O^{2-} ion and forms the ion pair, which in addition, acts as a charge carrier. The activation energy of the monovalent cation conduction in silica glass which has been estimated by Anderson and Stuart is indicated in Fig. 3, in this case, the solid line gives the values when the parameters $\gamma = 7$ and $G = 3 \times 10^{11}$ dyn cm^{-2} are used. In this model, it may be assumed that the value of γ is equal to the dielectric constant of the sample and it involves both the atomic polarization and the electronic polarization. For the monovalent cation, it is expected that the activation energy will decrease and then increase with increasing radius of the cation. According to this model, ions smaller than Na^+ have high activation energies because they have excessive binding energies, whereas ions larger than Na^+ have high activation energies because they induce excessive strain energies. By comparing the observed results in this work and the solid line indicated in Fig. 3, it seems that the correlation between the activation energy and the radius of the monovalent cation is qualitatively interpretable in terms of this model. But for the results obtained especially for the LiH- and LiLi-forms fired at 600° C or above, the activation energy determined in a higher temperature range is considerably lower than the expected value indicated by the solid line. Several reasons can be considered for this difference. One of the reasons may be the change of dielectric constant because the activation energy for the LiH- and LiLi-forms fired at 600° C or above is less than that for the NaNa- or NaH-forms. To define the variation of the dielectric constant of the bulk itself, complex impedance analysis was applied. In Fig. 5, the results

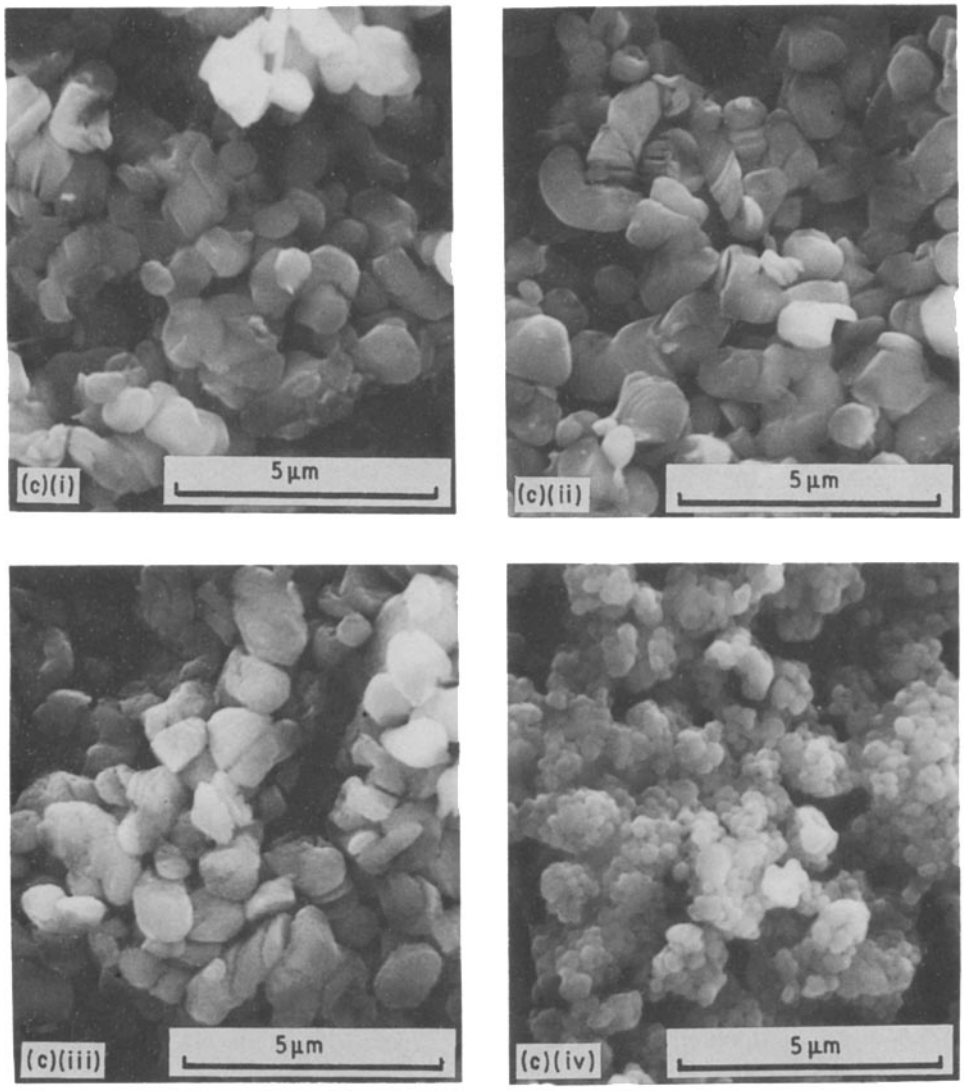

Figure 2 Continued.

observed in a frequency range 100 Hz to 100 kHz for the LiLi-form fired at 600° C are shown. In a lower temperature range, the high-frequency results are represented by depressed semicircles, all of which pass the origin and, at lower frequencies, a typical slanted vertical line is observed. By increasing the measuring temperature, the semicircle diminishes and only the line is observed. It seems that the semicircle reflects the bulk characteristics and the line the interfacial polarization and/or grain boundaries. Roughly speaking, the capacitance at 100 kHz reflects the bulk in a lower temperature range and the interfacial polarization and/or grain boundaries in a higher range.

In Fig. 6, the correlation between the capacitance and the measuring temperature is shown for the sample fired at 600° C. For NaNa-, KK- or RbRb-forms, the capacitance increases slightly with temperature, but for the LiLi-form, the correlation is more complex, i.e. the capacitance increases in two stages and two plateau regions are observed in which the capacitance observed in the temperature range below $\sim 300°$ C belongs in the semicircle in the complex impedance plot, while in a higher range, it belongs to the slanted line. The appearance of the second plateau suggests an increase in the dielectric constant of the bulk itself. For comparison, the characteristic temperature at the point at which a bend in the log σT–$1/T$ plot was observed is indicated by the arrow in Fig. 6. It seems that the increase in capacitance is comparable to the decrease in the activation energy in conduction. While it is difficult to determine exactly the dielectric constant of the bulk itself, the decrease in the activation energy with temperature for the LiH- and LiLi-forms is qualitatively interpretable in terms of the increase in the dielectric constant of the bulk itself. To determine the dielectric constant of the bulk itself, it is necessary to determine the depression angle and the characteristic frequency for the semicircles. In the frequency range used, good semicircles could not be obtained to determine these characteristics, except in some cases. For LiH- and LiLi-forms fired at 600° C or above, the sample obtained was composed of lithium dizirconium triphosphate and zirconium pyrophosphate. The dielectric constant of zirconium pyrophosphate which was prepared by heating the HH-form up to 900° C, is estimated to be ~ 10 and increases only slightly with temperature. Thus the distinct increase in the capacitance observed in a lower temperature range below $\sim 300°$ C may be caused by the lithium dizirconium triphosphate behaviour, i.e.

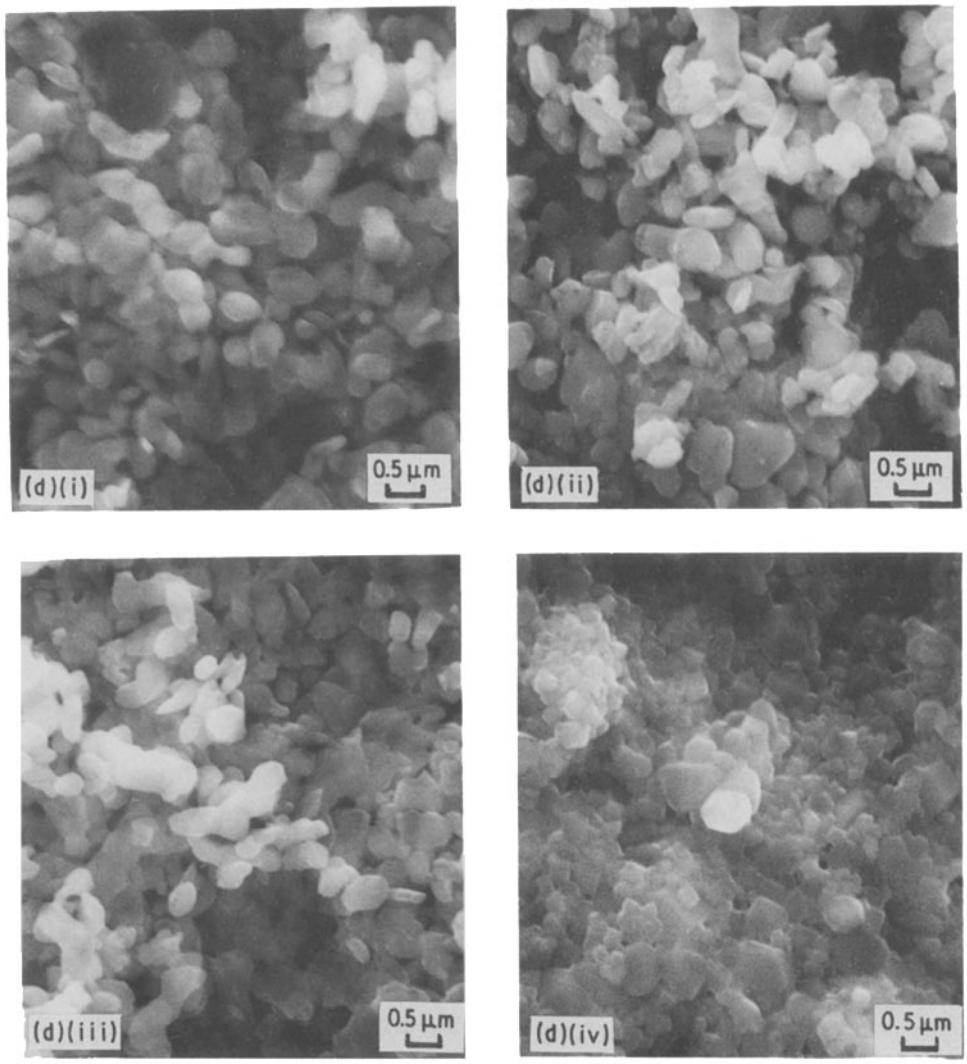

Figure 2 Continued.

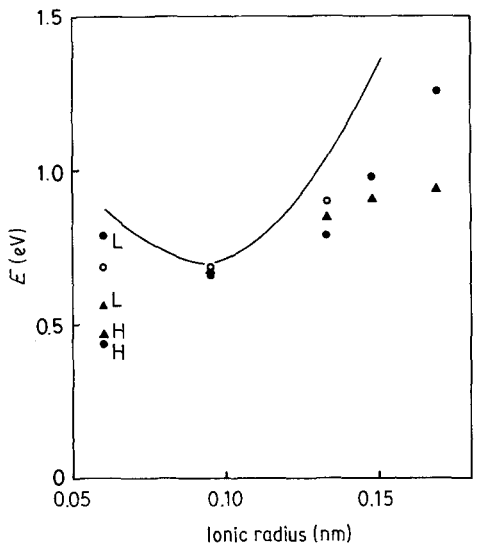

Figure 3 Correlation between activation energy in conduction and monovalent cation radius for fully exchanged samples. Firing temperature: (○) 300° C, (▲) 600° C, (●) 900° C. L, H: measured in a lower and higher temperature range, respectively. (——) Value estimated by Anderson and Stuart [11].

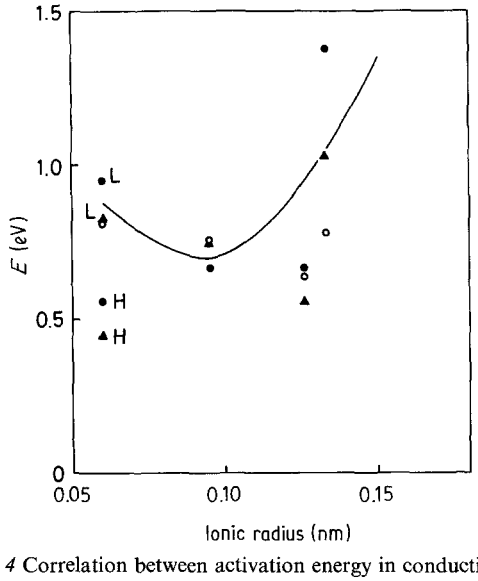

Figure 4 Correlation between activation energy in conduction and monovalent cation radius for half exchanged samples. Firing temperature: (○) 300° C, (▲) 600° C, (●) 900° C. L, H: measured in a lower and higher temperature range, respectively. (——) Value estimated by Anderson and Stuart [11].

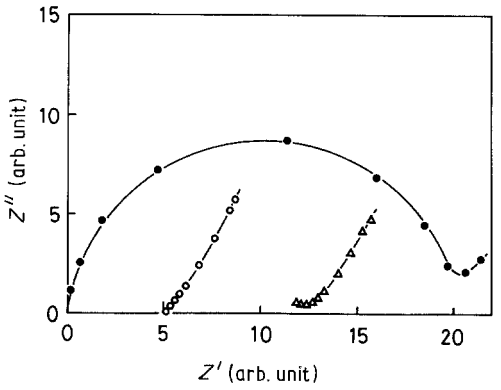

Figure 5 Complex impedance plot for LiLi-form fired at 600° C. Measuring temperature: (●) 30° C, (△) 210° C, (○) 420° C.

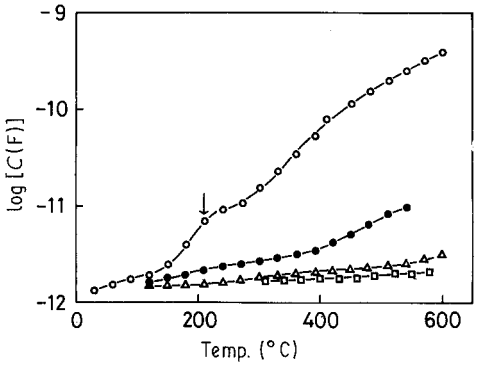

Figure 6 Correlation between capacitance at 100 kHz and measuring temperature for the sample fired at 600° C. (○) LiLi-form, (●) NaNa-form, (△) KK-form, (□) RbRb-form. Arrow denotes the temperature at which a bend is observed in log σT against $1/T$ plot.

the phase transition from monoclinic to rhombohedral. These observed results are specific for LiH- and LiLi-forms and no similar changes are observed for other alkali forms, while the formation of monoalkali dizirconium triphosphate is confirmed especially for half ion-exchanged forms fired at 600° C or above. To discuss in more detail the effects of ionic radius on the activation energy, it is necessary to determine exactly the dielectric constant and other characteristics, such as the shear modulus of the samples used.

References

1. A. CLEARFIELD, W. L. DUAX, A. S. MEDINA, G. D. SMITH and J. R. THOMAS, *J. Phys. Chem.* **73** (1969) 3424.
2. G. ALBERTI, R. BERTRAMI and U. CONSTANTINO, *J. Inorg. Nucl. Chem.* **38** (1976) 1729.
3. G. ALBERTI, U. CONSTANTINO and J. P. GUPTA, *ibid.* **36** (1974) 2109.
4. S. YAMANAKA, *ibid.* **42** (1980) 717.
5. M. CASCIOLA and F. FABIANI, *Solid State Ionics* **11** (1983) 31.
6. A. DYER and F. T. OCON, *J. Inorg. Nucl. Chem.* **33** (1971) 3153.
7. Y. SADAOKA and Y. SAKAI, *J. Mater. Sci. Lett.* **5** (1986) 731.
8. G. ALBERTI and U. CONSTANTINO, *J. Chromatogr.* **102** (1974) 5.
9. A. LA GINESTRA, C. FERRAGINA and P. PATRONO, *Mater. Res. Bull.* **14** (1979) 1099.
10. D. PETIT, Ph. COLOMBAN, G. COLLIN and J. P. BOILOT, *ibid.* **21** (1986) 365.
11. O. L. ANDERSON and D. A. STUART, *J. Amer. Ceram. Soc.* **37** (1954) 573.

Received 11 April
and accepted 7 September 1988